

---

---

# Atmospheric-Turbulence Compensation Experiments Using Cooperative Beacons

Daniel V. Murphy

■ Lincoln Laboratory recently completed the three-year Short-Wavelength Adaptive Techniques (SWAT) field program, designed to investigate the performance of adaptive optics in a variety of scenarios. This article describes the operation of the SWAT adaptive optics system working with cooperative beacons. Examples are presented of system operation in compensating star images and in propagating a compensated laser beam to a satellite.

**A**DAPTIVE OPTICS makes it possible to see through the atmosphere without suffering the resolution degradation caused by turbulence. Applications include the high-resolution viewing of exoatmospheric objects and the propagation of near-diffraction-limited laser beams to space. Astronomical objects and satellites are of obvious interest for high-resolution imaging. Potential applications for laser propagation include ground-to-space communications and the transmission of high-energy lasers to intercept ballistic missiles.

Adaptive optics systems require a reference light source, or beacon, to measure the turbulence-induced atmospheric aberrations. The most convenient arrangement is for the beacon to be located at the object of interest and shining down toward the adaptive optics system. In such cases the beacon is said to be cooperative. Cooperative beacons can be either man-made (e.g., a light source on a satellite) or natural (e.g., a star). Scenarios that do not provide for a beacon at the target are termed uncooperative; special techniques are required for using adaptive optics in such cases (see the article by Byron G. Zollars [1] in this issue).

This article describes the operation of the Short-Wavelength Adaptive Techniques (SWAT) system working with cooperative beacons. The SWAT system was installed in a beam director that has a 60-cm

aperture at the Air Force Maui Optical Station (AMOS) facility on the island of Maui, Hawaii. Located at an elevation of 10,000 ft at the top of the dormant volcano Haleakala (Figure 1), the site has the advantages of fairly low turbulence, good atmospheric transmission, and generally clear skies. The SWAT system was used to compensate the images of bright stars as well as to transmit a low-power, compensated laser beam to a satellite. Lincoln Laboratory conducted tests from May 1988 to mid-April 1991.

## Adaptive Optics System for Star Compensation

Compensation of star images to enhance astronomical observations was one of the first recognized applications for adaptive optics. A recent review of the field is provided in Reference 2. Although the SWAT system was configured on Maui for propagating a beam to a satellite rather than for astronomical observations, good compensated imaging could still be achieved by using some of the brightest stars as beacons.

The operation of an adaptive optics system in compensating the image of a star is illustrated schematically in Figure 2. In this configuration, the star itself serves as the beacon for the adaptive optics. Starlight is collected by the beam director (comprising a track-



**FIGURE 1.** Air Force Maui Optical Station (AMOS) and the University of Hawaii facilities located at the edge of the Mount Haleakala crater on Maui, Hawaii. AMOS is the large white complex on the left.

ing flat and telescope), is reflected off the fast-steering mirror and the deformable mirror, and is sensed both by the wavefront sensor and by a far-field camera that records the image. When the adaptive optics system does not apply any correction, the wavefront aberration imposed on the starlight by its passage through the atmosphere results in a jittering, distorted image in the camera. When the system does apply a correction, the conjugate of the aberration that the wavefront sensor measures is applied to the deformable and fast-steering mirrors so that the wavefront is flat after reflecting off the deformable-mirror surface. The far-field camera then sees a jitter-free, unaberrated image of the star.

The deformable mirror does not usually perform compensation of the tilt component of turbulence. As shown in Figure 2, the task is off-loaded to a separate fast-steering mirror to reduce the stroke requirement for the deformable mirror. In this configuration, the deformable mirror compensates only the tilt-removed phase, often referred to as the wavefront figure. Commands for the fast-steering mirror can be obtained either from the phase that the

wavefront sensor measures or from a separate sensor that measures only the overall wavefront tilt. The SWAT system utilizes a separate tracker so that tilt compensation (i.e., tracking) can be performed even when the wavefront sensor is not operating.

#### *Deformable Mirror*

The deformable mirror is the active wavefront corrector, and its characteristics largely determine the capability of the entire adaptive optics system. The important characteristics of a deformable mirror are the actuator density, influence function, stroke, and response speed. The actuator density is perhaps the dominant characteristic because it determines the highest spatial frequency of the aberration that the deformable mirror can compensate. The influence function—the shape of the mirror surface in the vicinity of an extended or retracted actuator—also plays a role in defining the spatial spectrum of the correction. The stroke of the mirror is the peak-to-peak displacement that an actuator can achieve. The stroke must be sufficient to apply corrections fully, both for turbulence and for static aberrations in the optics. Finally, the deformable mirror along with its

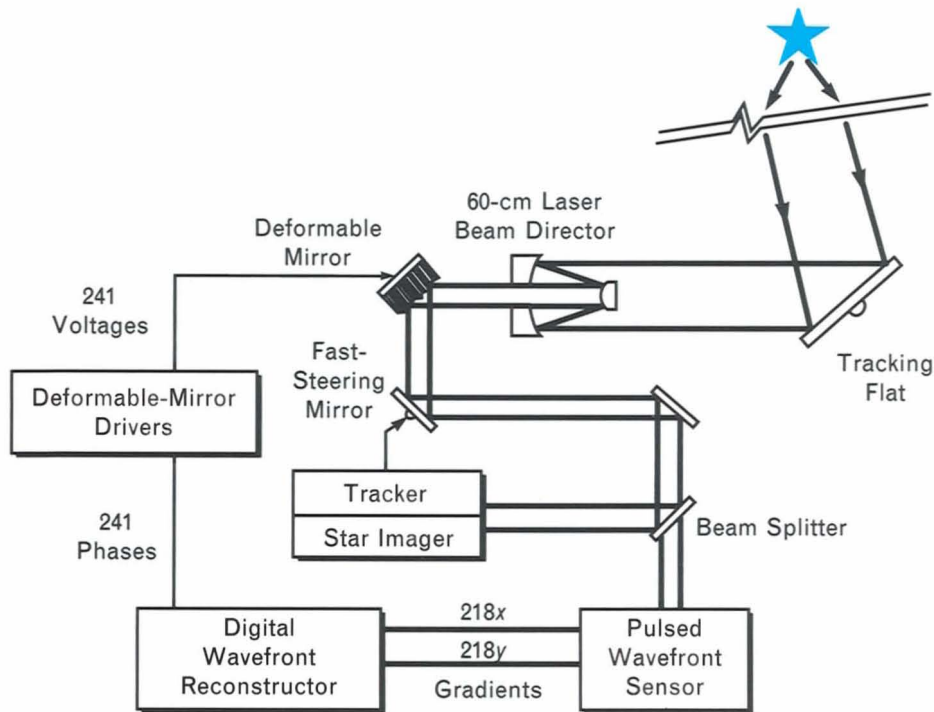


**FIGURE 2.** The Short-Wavelength Adaptive Techniques (SWAT) system performing cooperative-mode compensation of a star. In the cooperative mode, the beacon is located at the object of interest.

electronic drivers must be fast enough to keep up with the changing atmospheric turbulence; this response time requirement typically is on the order of milliseconds.

The SWAT deformable mirror, built by Litton Itek Optical Systems, uses low-voltage electrostrictive actuators that push and pull against a thin, reflective facesheet (Figure 3). The mirror has 241 actuators in a  $17 \times 17$  rectilinear array with the corners cut off. The actuator spacing is 7 mm at the mirror, which is equivalent to 3.3 cm in the atmosphere after magnification in the telescope portion of the beam director. The 3.3-cm actuator spacing is appropriate for near-diffraction-limited compensation of turbulence as strong as  $r_0 = 5$  cm, where  $r_0$  is the atmospheric coherence diameter (see the box "Derivation of Turbulence-Imposed Requirements for Adaptive Optics Components"). For an applied voltage of 300 V, the mirror has a maximum stroke of  $3.5 \mu\text{m}$ , which is more than ample to correct turbulence and optics aberrations. The rise time of the electronic drivers

and the mechanical resonances in the mirror structure itself determine the temporal characteristics of the deformable mirror. The SWAT deformable mirror is able to settle to a desired wavefront figure within a few hundred microseconds of a command. Figure 4 shows the mirror drive electronics.

#### Wavefront Sensor

It is difficult to build a sensor to measure the wavefront phase directly, so almost all sensors measure the local gradients of the wavefront in an array that is matched to the deformable-mirror actuators, as shown in Figure 5. Values of the phase at each actuator location are then obtained by calculating the phase from the gradients in a separate wavefront reconstructor.

The SWAT wavefront sensor (WFS) is based on the classic Hartmann test for examining optics. As shown in Figure 6, the sensor uses an array of lenslets to divide the incoming wavefront into subapertures, with the light in each subaperture brought to focus within a  $4 \times 4$  subarray of pixels on a charge-coupled

---



---

## DERIVATION OF TURBULENCE-IMPOSED REQUIREMENTS FOR ADAPTIVE OPTICS COMPONENTS

---



---

THE ESSENTIAL REQUIREMENTS for an adaptive optics system can be derived from the theoretical properties of turbulence-induced wavefront aberrations. As the following paragraphs show, expressions for quantities such as deformable-mirror and tilt-mirror strokes and wavefront-sensor measurement range have simple forms that involve the term  $(D/r_0)^{5/3}$ , where  $D$  is an aperture diameter (either the whole aperture or a subaperture) and  $r_0$  is the atmospheric coherence diameter [1]. The parameter  $r_0$  is a measure of the effect of turbulence on a wavefront; it is obtained by integrating the turbulence strength  $C_n^2$  over the line of sight through the atmosphere:

$$r_0^{-5/3} = 0.423k^2 \int_0^L C_n^2(z) dz,$$

where  $k$  is the wave number of light (equal to  $2\pi/\lambda$ ) and  $L$  is the distance from the receiver to the light source (the top of the atmosphere for a star).  $C_n^2(z)$ , known as the refractive-index structure function, is a measure of the turbulence strength and is strongly

dependent on altitude and local terrain. The parameter  $r_0$  has proven to be very useful because it has a simple physical interpretation: the resolution along a path characterized by  $r_0$  is limited by turbulence to approximately the resolution that would be obtained by a diffraction-limited aperture of diameter  $r_0$ . Values of  $r_0$  for visible light vary from about 20 cm at good astronomical sites to less than 5 cm. Thus, even though large ground-based telescopes with diameters up to 4 m can gather a lot of light, they can achieve no better resolution than telescopes with diameters of a few tens of centimeters.

In this article, wavefront aberrations are expressed in units of wavelengths of light for visible light ( $\lambda = 0.5 \mu\text{m}$ ). This convention is often a point of confusion because turbulence-induced aberrations are, to the first order, independent of wavelength. Turbulence creates variations in the optical path that are characterized in units of length, independent of the color of the light that passes through the atmosphere. The effect on the image, howev-

er, does depend on the wavelength. For example, turbulence may cause the optical-path lengths of two nearby rays to differ by  $1 \mu\text{m}$ . For visible light ( $\lambda = 0.5 \mu\text{m}$ ) this difference represents a 2-wave aberration and will severely degrade an image. But for light at  $10 \mu\text{m}$ , the difference represents an aberration of only 0.1 wave and will barely degrade an image at all. Thus the use of wavelength as a unit is convenient because it provides a subjective feel for the importance of the aberration at the wavelength of interest.

### Deformable Mirror

The difference between a turbulence-induced wavefront aberration and the best correction that can be applied by a deformable mirror with an array of discrete actuators is known as the fitting error. The spatial variance of the fitting error [2] is given simply by

$$\sigma_f^2 = \mu \left( \frac{d}{r_0} \right)^{5/3} \text{ waves}^2, \quad (\text{A})$$

where  $d$  is the inter-actuator spac-

device (CCD) detector. When the CCD is read out, the pixels from each subarray are processed with a centroid algorithm to determine the location of the focal spot. The displacement of the spot from the

center of the subarray is proportional to the average tilt, or gradient, of the portion of the wavefront in that subaperture.

It is worth emphasizing that the wavefront-sensor

ing and  $\mu$  is a constant that depends on the influence function of the mirror. For the SWAT system,  $d = 3.3$  cm (17 actuators across a diameter of 56 cm) and  $\mu = 8.7 \times 10^{-3}$  waves<sup>2</sup>. In a system intended to approach diffraction-limited compensation, it is generally desirable to have  $\sigma_f \leq \frac{1}{15}$  wave rms. Equation A predicts, then, that the SWAT system should be capable of correcting turbulence with a strength corresponding to  $r_0 \approx 5$  cm.

The stroke of a deformable mirror must be at least large enough to apply a correction equal to the peak-to-peak wavefront aberration. The variance of the uncompensated wavefront figure [3] is

$$\sigma_\phi^2 = 3.57 \times 10^{-3} \left( \frac{D}{r_0} \right)^{5/3} \text{ waves}^2,$$

where  $D$  is the overall diameter of the telescope aperture. As an approximate rule of thumb, the peak-to-peak phase aberration is about 5 times  $\sigma_\phi$  or about 2.2 waves for  $r_0 = 5$  cm. The stroke required to apply a 1-wave aberration is only  $0.25 \mu\text{m}$  because 1 wave is  $0.5 \mu\text{m}$  and the wavefront aberration resulting from reflection is twice the aberration of the surface of the mirror. Thus a

stroke of only  $0.55 \mu\text{m}$  is required to compensate turbulence of strength  $r_0 = 5$  cm.

### Wavefront Sensor

The strength of the turbulence and the size of a subaperture determine the required gradient measurement range of the wavefront sensor. The variance of the wavefront gradients caused by turbulence and measured within a subaperture of diameter  $d$  is

$$\sigma_g^2 = 0.170 \left( \frac{d}{r_0} \right)^{5/3} (\text{waves/sub-aperture})^2.$$

Again, with the rule of thumb that the extreme range of gradients is about five times the standard deviation, the required dynamic range for turbulence of strength  $r_0 = 5$  cm is  $\pm 0.75$  waves/subaperture.

### Fast-Steering Mirror

The required angular range of the fast-steering mirror can be estimated from the turbulence-induced tilt variance [3] given by

$$\sigma_\alpha^2 = 0.184 \left( \frac{D}{r_0} \right)^{5/3} \cdot \left( \frac{\lambda}{D} \right)^2 (\text{radians of tilt})^2.$$

For  $r_0 = 5$  cm, the maximum wavefront tilt is  $\pm 7 \mu\text{rad}$ , which requires a mechanical mirror tilt of  $\pm 3.5 \mu\text{rad}$ . The mechanical-tilt requirement is actually  $\pm 3.5 \mu\text{rad} \times 14.1 \approx \pm 50 \mu\text{rad}$ , where 14.1 is the magnification between the fast-steering mirror (beam diameter = 4.0 cm) and the 56-cm beam in the atmosphere.

It is easy to see why tilt is usually unloaded from the deformable mirror to a separate corrector. Driving a deformable mirror to a tilt of  $3.5 \mu\text{rad}$  would require a peak-to-peak stroke of  $3.5 \mu\text{rad} \times D \approx 2 \mu\text{m}$ . This requirement is larger than the stroke required to compensate the higher-order wavefront-figure aberration, and is uncomfortably close to the maximum stroke capability of the SWAT deformable mirror.

### References

1. D.L. Fried, "Limiting Resolution Looking Down through the Atmosphere," *J. Opt. Soc. Am.* 56, 1380 (1966).
2. D.P. Greenwood, "Mutual Coherence Function of a Wave Front Corrected by Zonal Adaptive Optics," *J. Opt. Soc. Am.* 69, 549 (1979).
3. D.P. Greenwood and D.L. Fried, "Power Spectra Requirements for Wavefront-Compensation Systems," *J. Opt. Soc. Am.* 66, 193 (1976).

measurements are independent of wavelength; in fact, the WFS works well with white light. The displacement of a focal spot at the detector plane is proportional to the average tilt of the portion of the wavefront within that subaperture—independent of wavelength. Thus the WFS actually measures an array of geomet-

ric wavefront tilts. For convenience, these tilts (or gradients) are usually expressed in units of optical path difference in wavelengths of light ( $\lambda = 0.5 \mu\text{m}$ ) across a subaperture.

An important characteristic of a WFS is the magnitude of the largest gradient that can be measured. In

the SWAT system, the maximum gradient is limited by the size of the  $4 \times 4$  subarray corresponding to each subaperture. If a focal spot moves too far off center, energy from the spot will spill into the adjacent subaperture and compromise the measurements in both subapertures. The SWAT WFS has a linear measurement range of  $\pm 1.4$  waves/subaperture, sufficient to measure turbulence and static-optics aberrations (see the box “Derivation of Turbulence-Imposed Requirements for Adaptive Optics Components”).

Another critical characteristic for a WFS that works with low signal levels is the sensor’s photon sensitivity, characterized by the measurement error as a function of light level. The variance of the gradient error for a Hartmann sensor with a 4-pixel centroid algorithm is

$$\sigma_g^2 = \frac{0.526}{\eta N} + \frac{6.09 \sigma_c^2}{(\eta N)^2} (\text{waves/subaperture})^2, \quad (1)$$

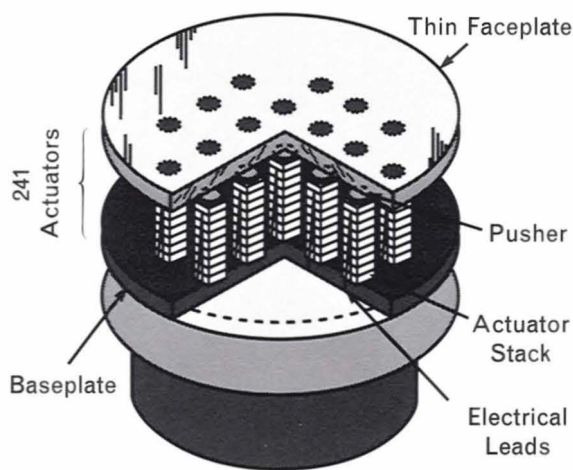
where  $N$  is the number of photons arriving at the detector per measurement interval per subaperture,  $\eta$  is the detector quantum efficiency, and  $\sigma_c$  is the read-out noise of the detector in electrons. The first term in Equation 1 is the photon shot noise, which is derived from the arrival statistics of the photons, and the second term is the noise that the detector im-

poses. Ideally, the overall noise would be determined by photon statistics, but in practice the detector noise dominates the low-light performance of the SWAT sensor.

The SWAT WFS utilizes  $64 \times 64$ , backside-illuminated CCD detectors developed at Lincoln Laboratory [3]. The detectors have an average quantum efficiency of about 80% over the wavelength band of 0.42 to 0.54  $\mu\text{m}$  transmitted by the optics, and the noise of the chips and readout electronics combined is 25 to 30 electrons per pixel at a readout rate of 4.2 Mpixels/sec. From Equation 1, these numbers predict that a single-measurement root-mean-square (rms) gradient noise of  $\frac{1}{15}$  wave/subaperture can be achieved with  $N \approx 1350$  photons. This photon flux corresponds roughly to the signal received from a bright star of visual magnitude zero with the WFS running at a 2-kHz frame rate.

In addition to the optics and detectors described above, the WFS has processing electronics for performing the centroid calculation and for applying the appropriate calibration factors to convert the raw camera data to gradients. The time required to frame, or cycle, the cameras and output the entire serial stream of gradients is approximately 225  $\mu\text{sec}$ .

A thorough description of the design and performance of the SWAT WFS can be found in the



(a)



(b)

**FIGURE 3.** Deformable mirror: (a) schematic representation of a continuous-facesheet deformable mirror, and (b) photograph of the SWAT deformable mirror.



**FIGURE 4.** SWAT control electronics for adaptive optics. From right to left, the racks contain (1) driver electronics for the deformable mirror, (2) a wavefront reconstructor (bottom) and a real-time display for wavefront-sensor data (top), (3) electronics for data formatting and overall system control, and (4) a video display for the charge-coupled device (CCD) far-field camera.

article by Herbert T. Barclay et al. [4] in this issue.

#### *Reconstructor*

A gradient measured in the array shown in Figure 5 can be approximated as the difference of the phase values at the two nodes it connects. In that case, the wavefront measurement can be modeled as the matrix operation

$$\mathbf{g} = \mathbf{A}\boldsymbol{\phi} + \mathbf{n}, \quad (2)$$

where  $\mathbf{g}$  is a 436-element vector comprising the measured gradients (there are 218x and 218y gradients),  $\mathbf{A}$  is a 436 × 241-element differentiation matrix,  $\boldsymbol{\phi}$  is a 241-element vector of the values of the wavefront phase at the actuator locations, and  $\mathbf{n}$  is a vector representing the gradient measurement noise. Although Equation 2 cannot be solved uniquely for the phase because of the noise term, the equation can be

solved to find the best estimate of the phase in the least-squares sense [5]—the solution has the simple form

$$\hat{\boldsymbol{\phi}} = \mathbf{B}\mathbf{g}, \quad (3)$$

where  $\hat{\boldsymbol{\phi}}$  is an estimate of the phase and  $\mathbf{B}$  is a 241 × 436-element reconstruction matrix. Thus the reconstruction of the phase from the gradient measurements can be performed as a single matrix-multiplication operation.

The matrix multiplication is straightforward to implement, but high data rates are required to keep up with the maximum frame rate of the wavefront sensor. The phase reconstruction was performed in the SWAT system by a special-purpose digital processor [6] designed and built at Lincoln Laboratory (Figure 4). The processor has 241 parallel channels that correspond to the 241 phase nodes. Each channel uses commercially available multiplier/accumulator

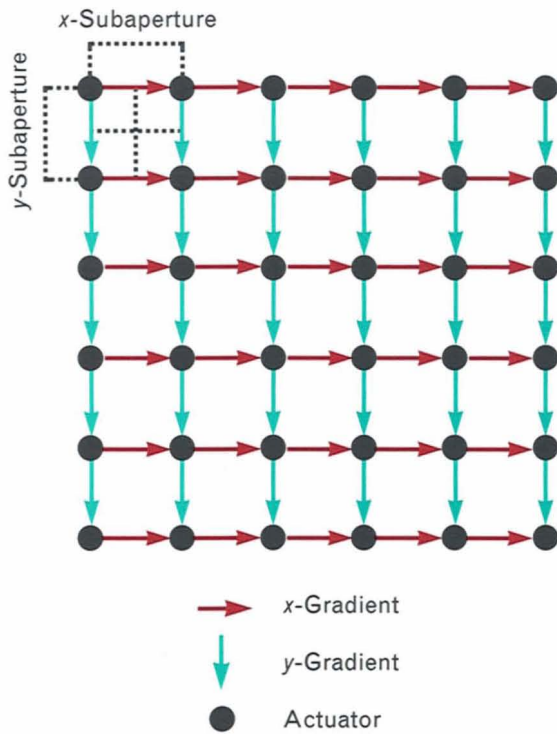


**FIGURE 5.** Layout of the  $x$ - and  $y$ -gradients measured by the wavefront sensor. Each gradient is averaged over a square subaperture. Separate detectors are used for the  $x$ - and  $y$ -gradients to permit the spatial offsetting of the  $x$ - and  $y$ -subapertures, as shown.

chips to calculate a weighted, linear sum of all input gradients, in which the weights are just the matrix elements from Equation 3:

$$\hat{\phi}_n = \sum \mathbf{B}_{n,i} \mathbf{g}_i$$

As the gradient values are clocked into the reconstructor, each value is multiplied by the appropriate matrix element read from memory and the value is then added to the cumulative sum. The reconstruction is complete on receipt of the last gradient from the wavefront sensor, so the pipeline delay is only a few cycles of the 5-MHz clock. Several different reconstruction matrices can be stored in memory at one time, allowing easy switching from, for example, reconstruction of the full phase to reconstruction of the wavefront figure.

### Tracking System

The tracking system compensates tilt fluctuations in-

duced by turbulence as well as by mechanical vibrations in the optical train. The essential components of the system are a tilt sensor, control electronics, and a fast-steering mirror. The principal characteristics are the angular range of the fast-steering mirror and the temporal response of the system.

The SWAT tilt sensor is a position-sensing photomultiplier tube (PMT) manufactured by Hamamatsu Corp. The sensor uses a  $12 \times 12$  grid of anode wires to resolve the position of a spot of light that is incident on the photocathode. When the PMT is used as a tracker, the spot is formed by focusing the beacon light onto the face of the tube. In effect, the PMT measures overall tilt much as a subaperture in the wavefront sensor measures the local wavefront gradient, but with a much wider measurement range because of the 12 anode wires. Depending on the configuration of the optics, the tracker field of view can be as large as  $150 \mu\text{rad}$ .

The SWAT fast-steering mirror, designed and built at Lincoln Laboratory, uses three piezoelectric actuators to provide two-axis tilt for a 2.5-inch mirror. The maximum angular range of the mirror is  $\pm 300 \mu\text{rad}$ , which corresponds to a range of  $\pm 20 \mu\text{rad}$  in the atmosphere after magnification in the optics. This range is well in excess of the  $\pm 3.5 \mu\text{rad}$  required for turbulence compensation, as derived in the box “Derivation of Turbulence-Imposed Requirements for Adaptive Optics Components.” The extra range is used to compensate mechanical vibrations and to pull in targets that are slightly off boresight.

The tracking system can be operated with a closed-loop bandwidth of either 225 or 600 Hz. The lower bandwidth is generally adequate for tracking stars; the higher bandwidth was provided for tracking satellites.

### Closed-Loop Operation of System

When a continuous beacon source is available, the adaptive optics system can be operated in the closed-loop mode. Tilt compensation is performed by simply closing the tracking servo loops. Wavefront-figure compensation is performed by repetitively framing the wavefront sensor at a high rate to provide values of the phase at the 241 actuator locations of the deformable mirror. The figure compensation is

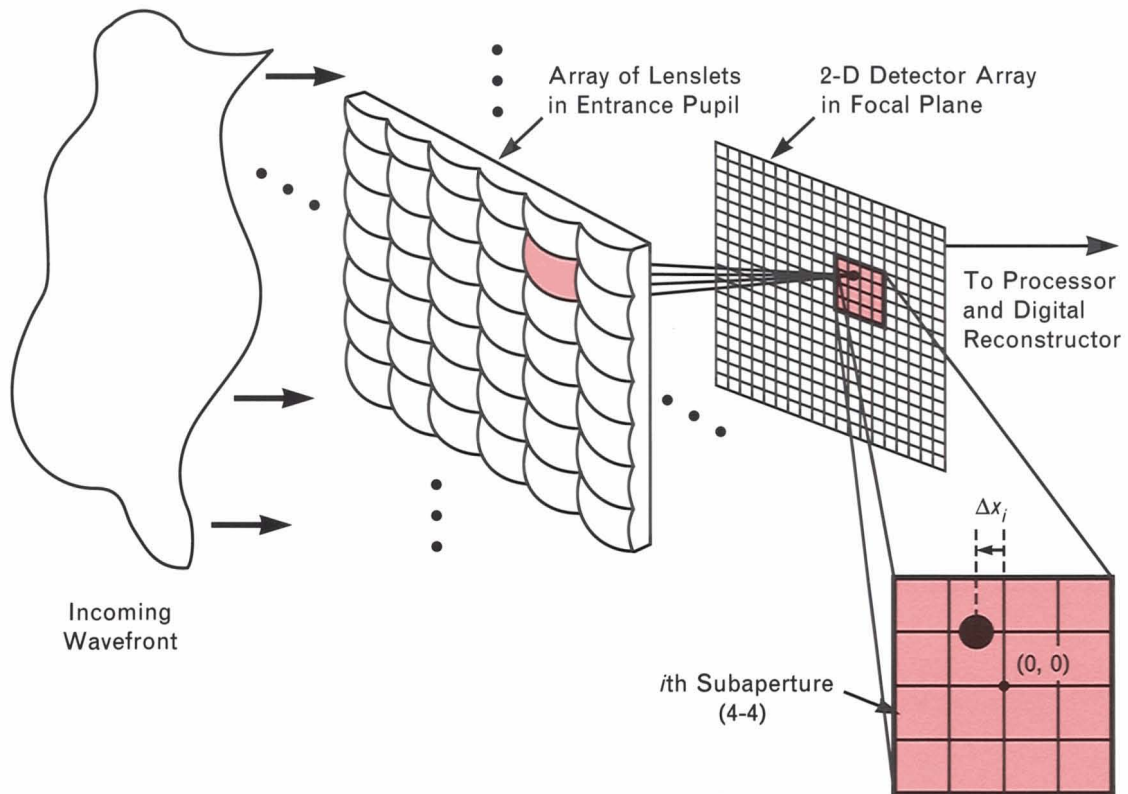


**FIGURE 6.** Principle of operation of a Hartmann wavefront sensor. The local phase gradient at the  $i$ th subaperture is proportional to  $\Delta x_j$ . The digital reconstructor computes the phase from the measured gradients.

applied by driving each actuator of the deformable mirror with its own servo loop to null the phase corresponding to that location. When the 241 parallel servo loops are closed, the deformable mirror is driven continuously to assume whatever shape is required to flatten the phase that the wavefront sensor measures. A servo bandwidth on the order of 100 to 200 Hz is required for the system to keep up with the changing atmospheric distortion when compensating a star.

Compensating the image of a bright star provides a good demonstration of the operation of the entire system. The performance of the tilt-compensation system is summarized in Figure 7, which shows the power spectral density of the single-axis tilt fluctuations that were measured by using a star as a beacon. The open-loop spectrum shows the turbulence-induced tilt disturbance in addition to a number of discrete lines caused by mechanical vibrations in the beam director. The closed-loop spectrum shows the residual error comprising both uncompensated tilt

and sensor measurement noise. In closed-loop operation, the cumulative rms jitter out to the servo bandwidth of 600 Hz was less than 50 nrad, which corresponds to a residual rms image jitter of about  $\frac{1}{20}$ th the diffraction-limited spot size for visible light. The high bandwidth and low residual jitter achieved by the tracking system ensured that there was essentially no tilt-induced smearing of the star image.

The system's figure-compensation capability is demonstrated in Figure 8, which shows compensated and uncompensated images of the star Sirius (visual magnitude  $-1.6$ ) at an elevation of  $51^\circ$ . The images were recorded by a  $64 \times 64$  CCD camera that was similar to the ones used in the wavefront sensor; the angular field of view of the camera was  $19 \mu\text{rad}$ . Coatings on the optical components limited the wavelength passband to  $0.42\text{--}0.54 \mu\text{m}$ . Because both images were recorded with the tracking loops closed, the degradation of the uncompensated image was caused entirely by aberrations in the atmosphere and system optics.

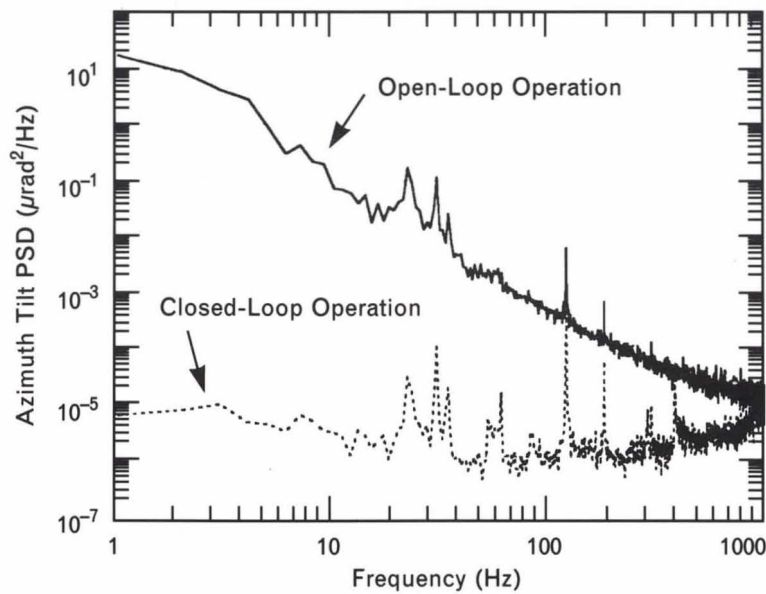


**FIGURE 7.** Power spectral densities (PSD) of single-axis tilt fluctuations measured from the star Sirius with the tilt servo loops open and closed. The cumulative jitter out to the 600-Hz servo bandwidth was 6  $\mu\text{rad}$  root mean square (rms) in open-loop operation, and 43 nrad rms in closed-loop operation.

The image of a point source can be characterized quantitatively by the Strehl ratio—the ratio of the peak intensity of the image to the peak intensity of a diffraction-limited image. The Strehl ratio can be

easily calculated from a compensated image if one assumes that the exposure contains all the energy of a diffraction-limited image, a reasonable assumption at least for compensated images. For the compensated

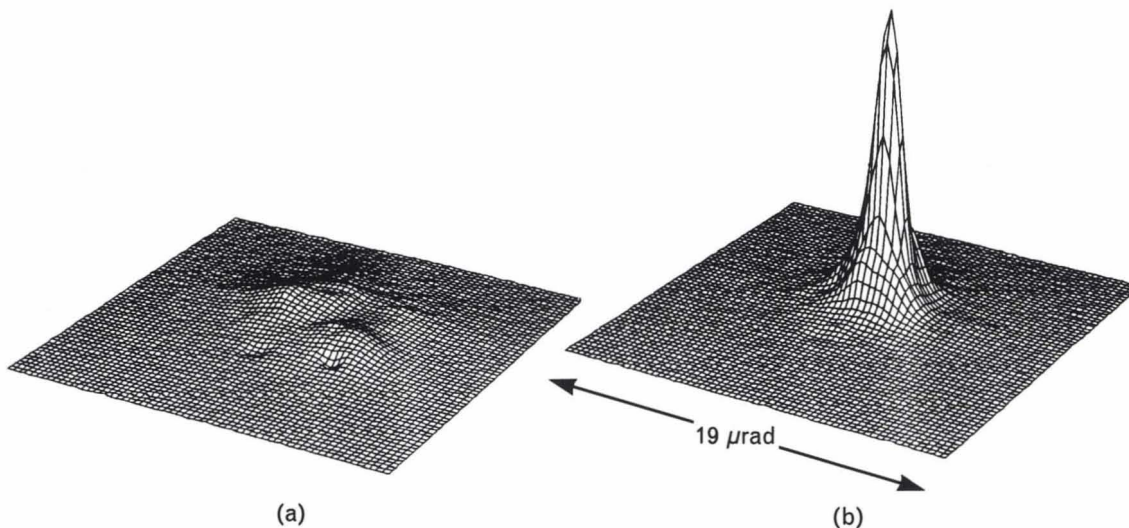


**FIGURE 8.** Images of the star Sirius with the figure-compensation loops (a) open and (b) closed. The tracking loops were closed for both images, and each image is the average of 50 exposures recorded over a 1-sec interval. The star elevation was 51°, and  $r_0$  (see the box "Derivation of Turbulence-Imposed Requirements for Adaptive Optics Components") was approximately 9 cm. The Strehl ratio was about 0.03 for the image in part a and about 0.3 for the image in part b. (The Strehl ratio is the ratio of the peak intensity of the image to the peak intensity of a diffraction-limited image.)

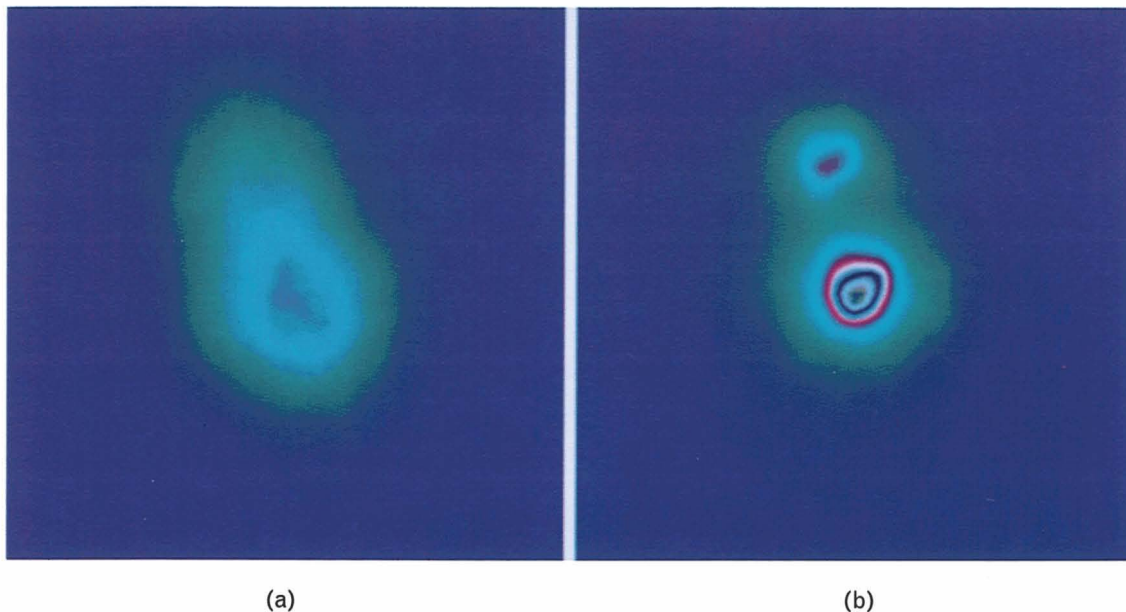


**FIGURE 9.** The binary star Castor: (a) uncompensated and (b) compensated images. The tilt and figure loops were both open for the uncompensated image and closed for the compensated image. The separation between the two stars is  $15 \mu\text{rad}$  (approximately 3.1 arc sec).

image in Figure 8, the Strehl ratio is 0.3; for the uncompensated image it is about 0.03. The principal factors that limit the compensated Strehl ratio are the fitting error (see the box “Derivation of Turbulence-Imposed Requirements for Adaptive Optics Components”), wavefront-sensor measurement noise, and residual phase fluctuations outside the correction bandwidth.

Figure 9 shows another compensated image, that of Castor—a binary star of visual magnitude 2.0 for which the separation of the two components is  $15 \mu\text{rad}$  (3.1 arc sec). An image with no compensation (Figure 9[a]), and one with tilt and figure compensation (Figure 9[b]) are shown; each image is the average of 50 frames collected over a 1-sec interval. Because Castor is much dimmer than Sirius, the compensation is nowhere near the diffraction limit. Nevertheless, the system easily resolved the two stars, which were clearly not resolved without any correction.

### Scoring-Beam Compensation

As mentioned earlier, the SWAT system was primarily designed to compensate an outgoing, low-power laser beam. This type of compensation can be accomplished

by bringing the laser beam, referred to as the scoring beam, into the optical path so that it reflects off the deformable and fast-steering mirrors on its way through the system and out the beam director. Compensation of the scoring beam works in the same way as compensation of a beacon image except that the correction is applied to the scoring beam *before* it encounters the atmospheric aberration rather than after. The precorrection applied to the scoring beam is exactly canceled by the aberrations experienced by the beam as it propagates through the atmosphere. Consequently, the scoring beam has a flat wavefront at the top of the atmosphere and continues on to the target as a diffraction-limited beam.

The effectiveness of scoring-beam compensation is best judged by examining the intensity profile of the beam in the far field. A convenient way to make such measurements was provided at the AMOS site by a trailer located about 150 m away from the beam director (Figure 10). The trailer was equipped with both a laser source to serve as the beacon and a  $100 \times 100$ -pixel solid state camera to record the image of the focused scoring-laser spot. Although propagation over a short horizontal path does not model all aspects of ground-to-space propagation, the setup



**FIGURE 10.** Site of the horizontal-path measurements at AMOS. The red line indicates the 146-m propagation path from the small dome that houses the laser beam director to the instrumented target trailer.

was a good test of system operation because the integrated turbulence strength over the 150-m path to the trailer was comparable to that for a vertical path to space.

In the horizontal-path tests, the beam director was pointed at the trailer and the trailer beacon was acquired in the wavefront sensor and far-field CCD camera. The scoring beam was then transmitted out of the beam director and detected by the trailer's solid state camera. Closing the adaptive optics loops (both tilt and figure) resulted in the simultaneous compensation of the beacon image and laser spot. Because the scoring-laser beam and beacon light traversed the same path through the turbulence, they experienced the same degree of correction by the adaptive optics, and they generally had similar Strehl ratios. Nevertheless, the compensated beacon image and scoring-laser spot were not identical. The theoretical diffraction-limited profiles for the two were different because the laser beam and beacon light had different near-field intensity profiles: the scoring beam had a Gaussian profile with a  $1/e^2$  diameter of 48 cm while light from the beacon uniformly filled the 56-cm aperture. In addition, instrumental artifacts in the imaging system

broadened the beacon image slightly.

An example of good compensation over the path to the target trailer is illustrated in Figure 11, which shows compensated images of the beacon and of the scoring-beam spot recorded simultaneously over a 1-sec interval. As expected, the calculated Strehl ratios for the two images are comparable. Figure 12 characterizes the two compensated images as well as a pair of uncompensated images that were recorded with the deformable-mirror loops open but the tracking loops still closed. These figures, known as power-in-bucket plots, show the total power that would be collected within a circular "bucket" of a given radius centered on the image. It is easy to see qualitatively that the adaptive optics system dramatically decreased the spread of energy in both the beacon image and at the focus of the scoring laser. The expected difference in the shapes of the two images is readily apparent in the diffraction-limited and compensated curves.

### **Propagation to a Satellite**

One of the principal goals of the SWAT program was to propagate a compensated laser beam to a low-

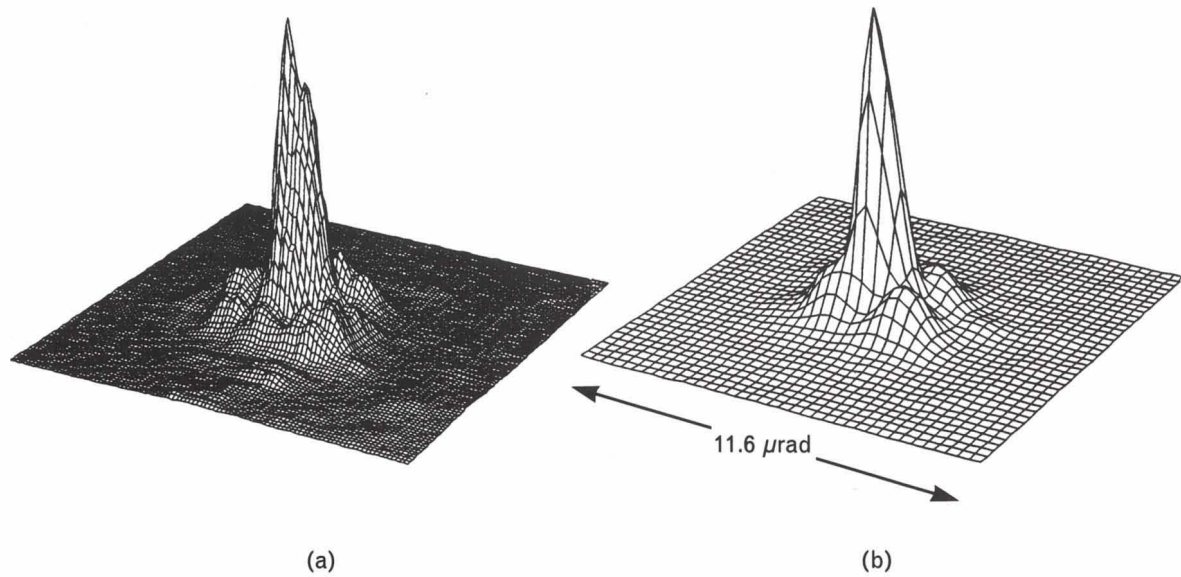


**FIGURE 11.** Compensated profiles of the (a) scoring beam and (b) beacon image recorded simultaneously for propagation over a horizontal path. Each profile has been averaged over 1 sec. The value of  $r_0$  was about 5 cm and the Strehl ratio for both images was about 0.5.

earth-orbiting satellite. Ground-to-space propagation of a compensated scoring beam was first demonstrated in 1985 as part of Lincoln Laboratory's Atmospheric-Compensation Experiment (ACE), but the slew rate of a low-orbit satellite is significantly higher than that of the sounding rockets used as targets in the ACE program. Propagation to a satellite, there-

fore, placed a greater burden on the adaptive optics because it demanded a faster temporal response.

The setup for transmitting a scoring beam to a satellite (Figure 13) was similar to that used for star compensation except for the addition of the instrumented satellite and a visible laser beam (in addition to the scoring beam) to illuminate a retroreflector

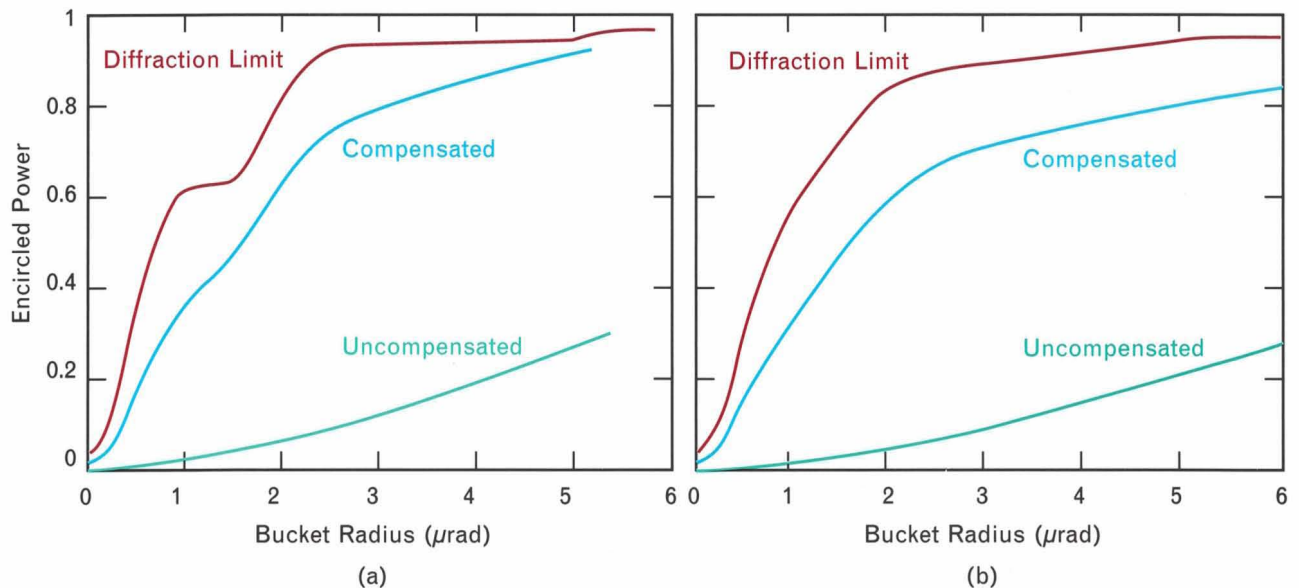


**FIGURE 12.** Power-in-bucket curves for the compensated profiles from Figure 11, the corresponding uncompensated profiles, and the theoretical diffraction-limited profiles for the (a) scoring beam and (b) beacon image. The curves show the total power that would be collected within a circular "bucket" of a given radius centered on the image.

beacon on the satellite. The experiment was performed by first acquiring the satellite on the boresight of the beam director, and then transmitting the beam from the retro-illuminating laser to irradiate the retro-reflector on the satellite. The laser light reflected from the retroreflector served as the beacon for the tracking system and for the adaptive optics. Closing the tracking and deformable-mirror servo loops resulted in a compensated image of the beacon in the far-field CCD imager. At the same time, closing the loops also resulted in compensation of the outgoing scoring beam, which could then propagate to the satellite as a

near-diffraction-limited beam. A detector array on the satellite was used to measure the profile of the scoring beam in order to characterize the degree of the compensation. The data from the satellite were telemetered to the ground and made available for display in real time.

The target satellite used for the ground-to-space phase of the SWAT program was designed and built specifically by the Naval Research Laboratory to measure the intensity profiles of ground-based laser beams. The satellite, known as the Low-Power Atmospheric-Compensation Experiment (LACE), was launched

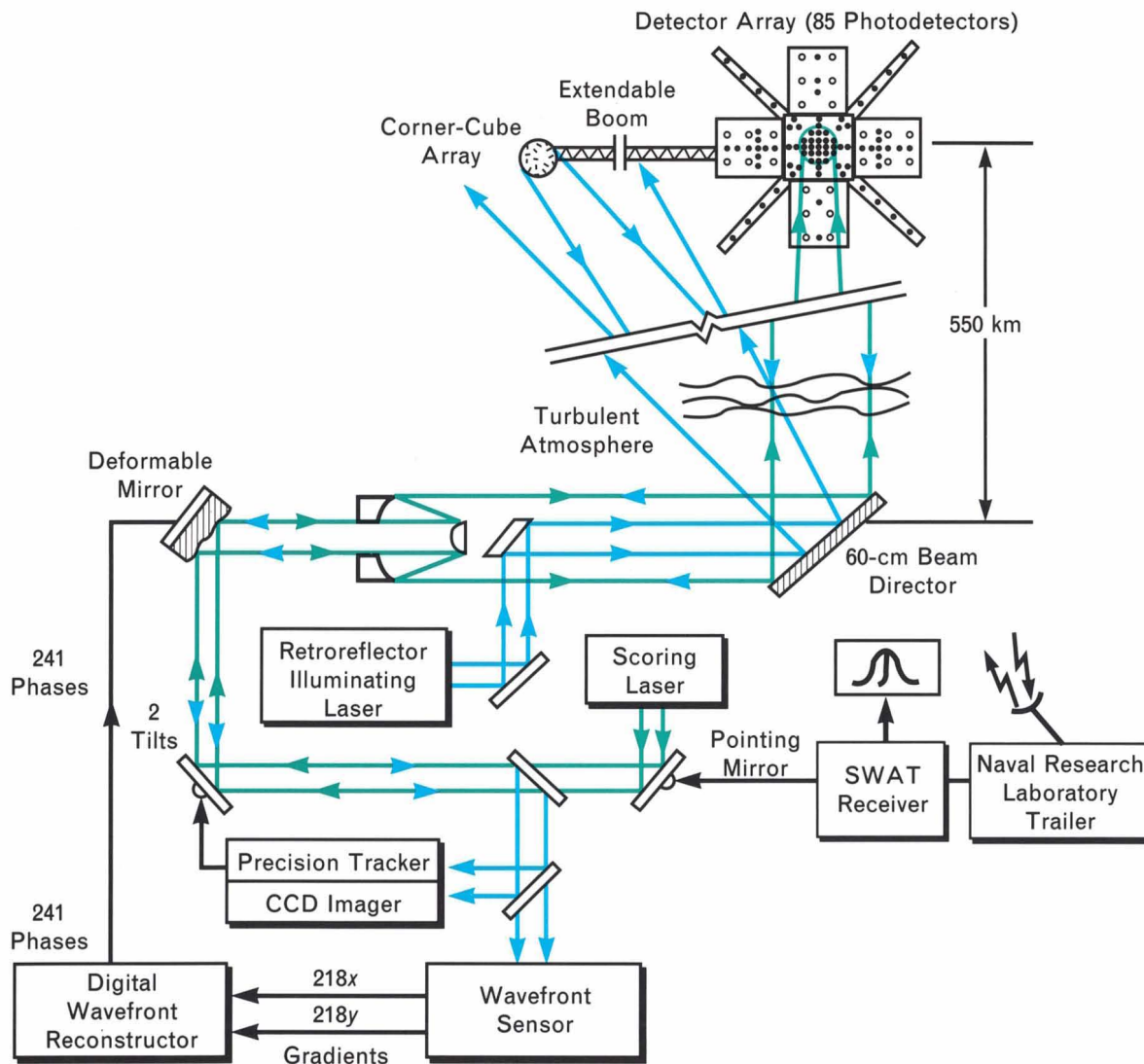


**FIGURE 13.** The SWAT adaptive optics system propagating a laser beam to the Low-Power Atmospheric-Compensation Experiment (LACE) satellite. Equipment specific to the satellite experiment were the satellite itself, the receiver for the telemetered data, and the retro-illuminating laser.

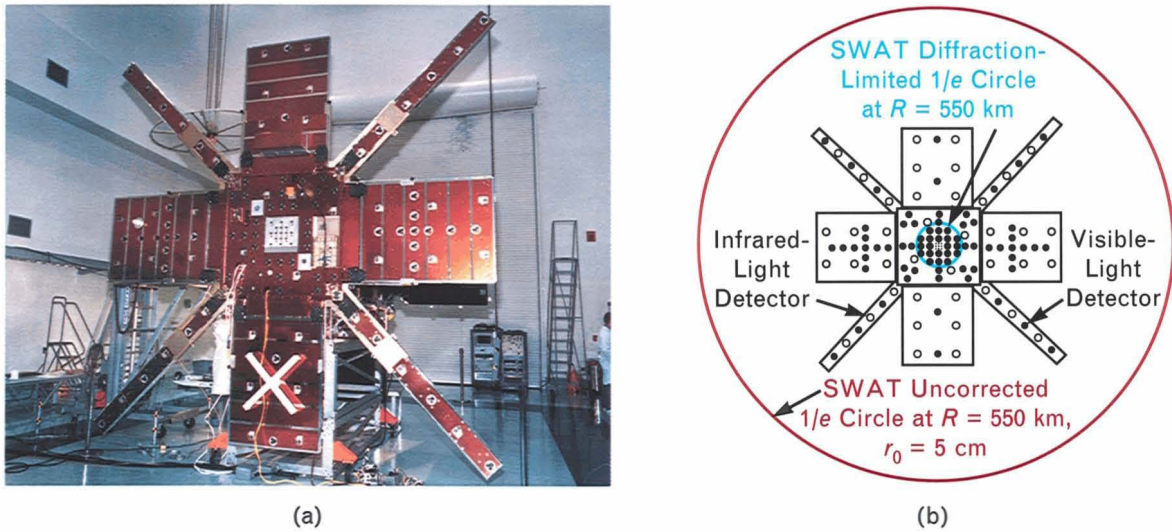


FIGURE 14. The detector array on the LACE satellite: (a) photograph and (b) diagram.

into a 547-km circular orbit with a  $43^\circ$  inclination in February 1990. (Note: A  $0^\circ$  orbit circles the equator; an orbit with a  $90^\circ$  inclination goes over the poles.) The features of the satellite most important for adaptive optics experiments were the retroreflector beacon and the detector array.

The LACE satellite used a retroreflector as a beacon to avoid the large power load that would have been imposed on the satellite by an active source such as a laser or lamp. A retroreflector is an optical prism with the property that an incident ray is reflected back on itself over a moderate range of incidence angles. Thus, when irradiated by a laser beam fired from the ground, a retroreflector acts like a highly directional source pointed directly back at the site. As long as the retroreflector is small enough so that it acts like a point source, atmospheric aberrations experienced on the uplink leg do not appear on the phase front of the return beam, and the wavefront received at the adaptive optics system has only the downlink aberrations imposed on it.

The angular acceptance of a large retroreflector is about  $30^\circ$  full width at half maximum, so a single retroreflector could be used as a beacon only if pointed at the ground site to within  $\pm 15^\circ$ . Because the LACE satellite is nadir-pointing and passively stabilized by gravity, this condition would occur only when the satellite was nearly overhead. Consequently, the LACE

retroreflector was designed to be an array of small, 1-inch-diameter retroreflectors mounted at various angles to provide a good return signal for elevation angles from  $90^\circ$  (when the satellite was directly over the ground site) down to  $45^\circ$ .

The retroreflector array was mounted at the end of a boom that could be extended to the correct point-ahead distance from the detector array before each pass of the satellite over the ground site (see the box "Point-Ahead Anisoplanatism"). For an overhead pass, the required boom length was 86 ft; for a low pass with a maximum elevation of only about  $50^\circ$ , the required boom length was about 110 ft.

The light source for illuminating the retro-array beacon was a CW Ar-ion laser mounted in the beam-director dome. This laser was tuned to a different wavelength than that of the scoring beam so that it would not be sensed by the detector array on the satellite. The beacon laser was transmitted as a small-diameter beam out of the central obstruction of the beam-director telescope (Figure 13). Because the diameter of the beam was only 2.5 cm at the beam director, diffraction spread the beam to a diameter of about 15 m at the satellite, making it relatively easy to hit the retroreflector array. In addition, an active pointing system with a bandwidth of a few hertz made small pointing adjust-

## POINT-AHEAD ANISOPLANATISM

TO BE COMPENSATED effectively, the outgoing laser beam must traverse the same column of atmosphere measured by the wavefront sensor. If the laser and beacon paths do not coincide exactly, the precorrection that the deformable mirror applies to the laser beam will not fully cancel out the atmospheric aberrations actually experienced by the beam, and the correction will be degraded. Errors resulting from imperfect overlap of the two atmospheric paths are known as anisoplanatism errors [1].

A common example of this type of error is angular anisoplanatism, which is caused by mispointing of the scoring laser from the beacon path. Angular anisoplanatism can also degrade a compensated image if the object being viewed is angularly offset from the beacon, in which case the rays that form the image do not traverse the same atmospheric path as do the beacon rays. This latter scenario may occur in astronomical applications in which one is

interested in viewing dim objects in the vicinity of a bright beacon star.

The amount that anisoplanatism degrades the compensation depends on the mismatch between the paths and on the turbulence conditions. For angular anisoplanatism, the mismatch is characterized by the angular pointing error, and the turbulence is characterized by the isoplanatic angle  $\theta_0$ . The definition of  $\theta_0$  contains an integral over the  $C_n^2$  profile similar to that for  $r_0$  (see the box "Derivation of Turbulence-Imposed Requirements for Adaptive Optics Components"), but with a range-dependent weight:

$$\theta_0^{-5/3} = 2.91k^2 \int_0^L z^{5/3} C_n^2(z) dz.$$

The  $z^{5/3}$  term emphasizes the contribution of turbulence at long ranges, where the linear separation of the two angularly divergent paths is greatest. For pointing errors less than  $\theta_0$  the beam is said to be within the isoplanatic

patch and the degradation is mild. The isoplanatic angle at visible wavelengths for vertical propagation through the atmosphere can vary from a few microradians to more than 20  $\mu\text{rad}$ . The relatively small value of  $\theta_0$  for visible light makes it impractical to apply cooperative-mode adaptive optics to astronomy because only an insignificant portion of the sky is covered by (i.e., within an isoplanatic patch of) stars bright enough to serve as beacons.

Angular anisoplanatism is an important potential error for ground-to-satellite adaptive optics applications; in that context, it is known as point-ahead anisoplanatism. The error arises because hitting a moving target such as a satellite requires the laser beam to be pointed ahead of the apparent target position by the point-ahead angle  $\theta_{pa} = 2v_{\perp}/c$ , where  $v_{\perp}$  is the speed of the satellite perpendicular to the line of sight, and  $c$  is the speed of light (Figure A). Point-ahead anisoplanatism degrades the correction because the scoring

elements to the laser beam to maximize the return signal from the retroreflector.

The detector array comprised 85 discrete Si photodetectors distributed in a 2-dimensional array (Figure 14). To enable the estimation of the total power received at the satellite, each detector was radiometrically calibrated over a range of  $1.0 \times 10^{-7}$  to  $5 \times 10^{-3}$

W/cm<sup>2</sup>. The wide dynamic range ensured that the array could measure the beam both with and without adaptive optics compensation. The entire array was sampled, or read out, at a 1-kHz rate, and the data were telemetered to the ground for recording and real-time display. The display allowed the operators to tell when the beam was hitting the satellite and to

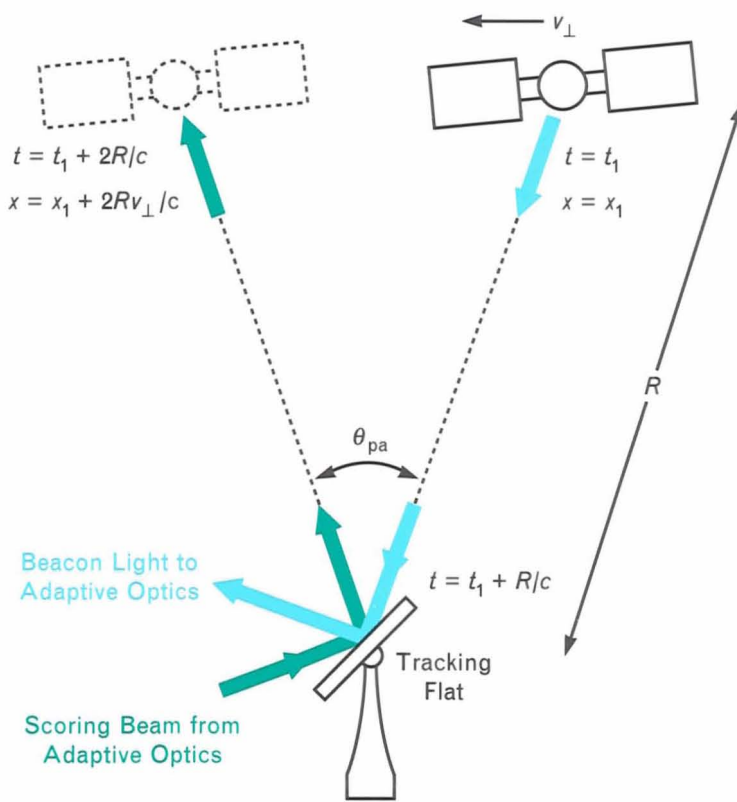


**FIGURE A.** Point-ahead angle  $\theta_{pa}$  of scoring beam fired at a satellite. The satellite moves perpendicular to the line of sight with speed  $v_{\perp}$  and emits a beacon pulse at time  $t_1$ . The transmitter on the ground receives the signal after a transit time of  $R/c$ , where  $c$  is the speed of light. The system on the ground then emits a scoring beam pulse that travels to the satellite and arrives after another transit delay of  $R/c$ . By that time, the satellite has moved a distance  $\Delta x = 2(R/c)v_{\perp}$ , so the scoring beam must be pointed ahead of the beacon arrival line of sight by  $\theta_{pa} = \Delta x/R = 2v_{\perp}/c$ .

beam must be angularly offset by  $\theta_{pa}$  from the atmospheric path of the beacon light coming down from the satellite. For a satellite in a 500-km orbit,  $\theta_{pa}$  is about  $50 \mu\text{rad}$  so the scoring beam is pointed well outside the isoplanatic patch and the degradation is severe.

The error caused by point-ahead anisoplanatism can be avoided by positioning the beacon ahead of the scoring-beam's aim point by an angle equal to  $\theta_{pa}$ . This adjustment would allow the scoring beam to be fired precisely through the column of atmosphere sampled by the beacon and still be able to hit the satellite. Such an approach was taken in the Low-Power Atmospheric-Compensation Experiment (LACE) in which a leading boom was used to position the retroreflector the appropriate distance ahead of the detector array (see Figure 13 in the main text).

*Reference*

1. D.L. Fried, "Anisoplanatism in Adaptive Optics," *J. Opt. Soc. Am.* 72, 52 (1982).

judge the effectiveness of the compensation. The real-time data were also used to drive a very-low-bandwidth pointing loop that kept the scoring beam centered on the array, thereby making the most efficient use of the relatively dense detector spacing at the center of the array.

Satellites with high slew rates impose an additional temporal bandwidth requirement on the adaptive op-

tics system beyond the requirements for star compensation. As far as adaptive optics applications are concerned, wind is the dominant factor that determines the dynamics of atmospheric turbulence. It is assumed that the turbulence aberrations are "frozen" in layers in the atmosphere, and that each layer is simply blown across the beam. The wind may be either the natural wind blowing across the beam or

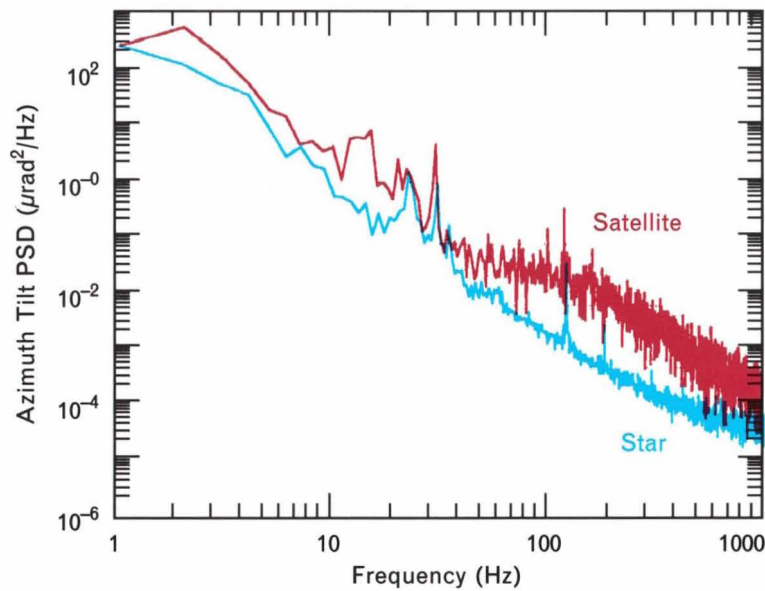


**FIGURE 15.** Open-loop power spectral densities (PSD) of single-axis tilt fluctuations measured from the satellite retroreflector beacon and from a star. Note the increased high-frequency power in the satellite spectrum.

the pseudowind generated by sweeping the beam through the atmosphere. For a slew rate of 10 mrad/sec, which is appropriate for the LACE satellite, the pseudowind speed at a range of 5 km, for example, is 50 m/sec—quite a bit higher than the speed of natural winds.

The effect of the high slew rate can be readily observed in the spectrum of the tilt fluctuations measured by the tracker with the tilt compensation loops open. Spectra measured on different nights with a star beacon and the LACE retroreflector beacon are plotted in Figure 15. Because the turbu-

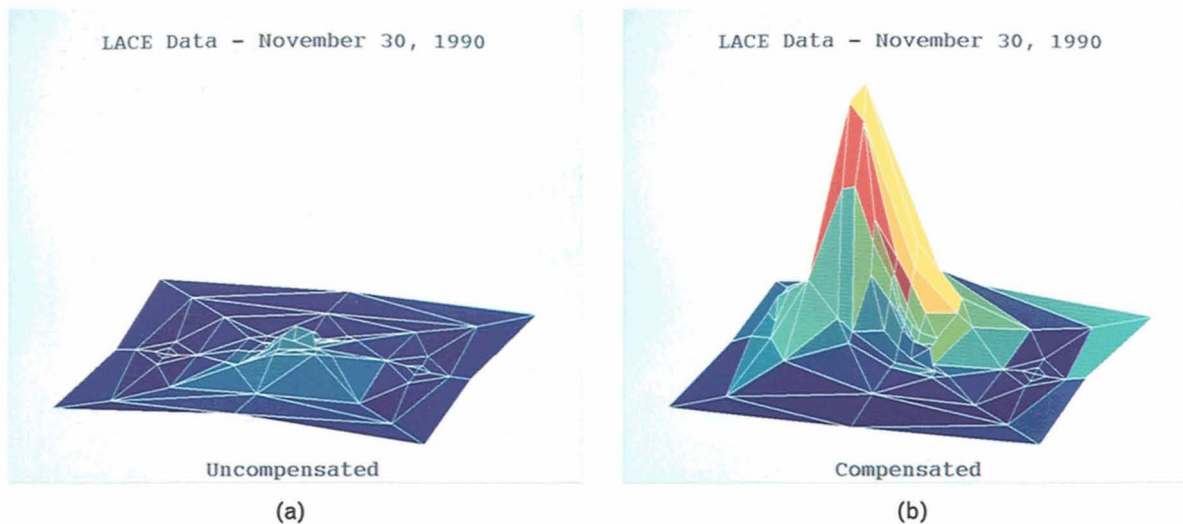


**FIGURE 16.** SWAT atmospheric-compensation experimental results: (a) uncompensated and (b) compensated scoring beam profiles measured at the LACE satellite. The elevation was 85°, and  $r_0$  was about 9 cm.

lence was somewhat stronger on the night the satellite tracking data were recorded, the overall spectrum for the satellite is higher than that for the star. Nevertheless, it is easy to see a disproportionate increase in tilt at high frequencies for the satellite beacon. For this reason, the tracking system was designed for closed-loop operation with a bandwidth of 600 Hz. Similar considerations apply for the figure-compensation loops.

Compensation experiments were performed with the LACE satellite over a 14-month period that began shortly after launch of the satellite (February 1990) and ended at the conclusion of the SWAT program (April 1991). Nighttime passes that were visible from AMOS and that had an elevation of at least  $45^\circ$  were candidates for tests. On average, there were about 20 such passes per month, although not all were scheduled for SWAT experiments. The duration of a pass from an elevation of  $45^\circ$  ascending to  $45^\circ$  descending was 2 to  $2\frac{1}{2}$  min.

The quantitative results of the satellite tests cannot be presented in this article, but Figure 16, which shows open- and closed-loop scoring-beam profiles measured at the satellite, at least gives a qualitative demonstration of the scoring-beam compensation. The profiles are plotted so that each vertex in the grid corresponds to a detector in the array on the satellite. The profiles appear a little coarse because of the relatively sparse sampling performed at the satellite. Nevertheless, it is easy to see the concentration of beam energy that occurred when the compensation was applied.

### Conclusion

The ability of adaptive optics systems to compensate for atmospheric turbulence by using cooperative beacons is by now well established. Previous experiments performed as part of Lincoln Laboratory's Atmospheric-Compensation Experiment (ACE) demonstrated propagation of a low-power laser beam to an aircraft and to sounding rockets. The ACE results have been complemented by the recent Short-Wavelength Adaptive Techniques (SWAT) tests,

which demonstrated high-bandwidth tracking and near-diffraction-limited compensated imaging of stars, as well as propagation of a compensated laser beam to a low-orbit satellite having a high slew rate. Taken together, these experiments provide a good base of experimental data for a variety of applications and a wide range of atmospheric conditions.

### Acknowledgments

The design, development, and operation of the SWAT adaptive optics system required the work of many people at Lincoln Laboratory. In particular, Robert Kramer was the original system engineer; Alden Marshall, Pete Rossini, Pete Smith, and Irv Wigdor developed the tracking system; Bert Willard designed the optical layout; Jim Mooney designed the wavefront reconstructor; Jon Twichell and Herb Barclay developed the wavefront sensor; Brian Player and Greg Rowe developed the display for the LACE data; Jan Herrmann, Ron Parenti, and Rich Sasiela provided the theoretical analysis; and Dan Page and Byron Zollars assisted in conducting the experiments.

This work was supported by the Strategic Defense Initiative Organization.

---



---

## REFERENCES

1. B.G. Zollars, "Atmospheric-Turbulence Compensation Experiments Using Synthetic Beacons," in this issue.
2. J.W. Hardy, "Adaptive Optics—A Progress Review," *Proc. SPIE* 1542, 2 (1991).
3. J.C. Twichell, B.E. Burke, R.K. Reich, W.H. McGonagle, C.M. Huang, M.W. Bautz, J.P. Doty, G.R. Ricker, R.W. Mountain, and V.S. Dolat, "Advanced CCD Imager Technology for Use from 1 to 10000 Å," *Rev. Sci. Instr.* 61, 2744 (1990).
4. H.T. Barclay, P.H. Malyak, W.H. McGonagle, R.K. Reich, G.S. Rowe, and J.C. Twichell, "The SWAT Wavefront Sensor," in this issue.
5. J. Herrmann, "Least-Squares Wave Front Errors of Minimum Norm," *J. Opt. Soc. Am.* 70, 28 (1980).
6. R.J. Sasiela and J.G. Mooney, "An Optical Phase Reconstructor Based on Using a Multiplier-Accumulator Approach," *Proc. SPIE* 551, 170 (1985).



**DANIEL V. MURPHY** received a B.A. degree in physics from Amherst College and a Ph.D. degree in engineering and applied science from Yale University. Dan is a staff member in the High-Energy-Laser Beam Control and Propagation Group, where his focus of research has been in adaptive optics.